

## Digital Communication Using Self-Synchronizing Chaotic Pulse Position Modulation

Nikolai F. Rulkov, Alexander R. Volkovskii, Michail M. Sushchik,  
Lev S. Tsimring, and Lucas Illing

**Summary.** We review a new approach to communication with chaotic signals based upon chaotic signals in the form of pulse trains where intervals between the pulses are determined by chaotic dynamics of a pulse nary information is modulated onto this carrier by the pulse position modulation method, such that each pulse is either left unchanged or delayed by a certain time, depending on whether 0 or 1 is transmitted. By synchronizing the receiver to the chaotic-pulse train we can anticipate the timing of pulses corresponding to 0 and 1 and thus can decode the transmitted information. Based on the results of theoretical and experimental studies we discuss the basic design principles for the chaotic-pulse generator, its synchronization, and the performance of the chaotic-pulse communication scheme in the presence of channel noise and filtering.

### 2.1 Introduction

In the last two decades intensive studies of chaotic behavior have produced various methods for controlling chaos and ideas for its possible applications. Chaos found in nonlinear electrical circuits [1–4] and lasers [5–11] provides means for generation of chaotic signals that can potentially be used as carriers for information transmission. The simplicity of chaos generators and the rich structure of chaotic signals are the two most attractive features of chaos that have caused a significant interest in possible utilization of chaos for communication.

Because the chaotic signal is nonperiodic, it cannot be stored in the receiver as a reference in order to achieve coherent detection of the transmitted signal. To overcome this problem, in some of the proposed communication schemes, the original chaotic waveform is transmitted along with the modulated signal (transmitted reference scheme) either using a separate channel or using time division [12]. Thus, a reliable detection can be achieved at the expense of at least 3 dB of the signal-to-noise ratio. In another approach, a chaotic reference is regenerated at the receiver using the phenomenon of chaos

synchronization [13]. It was shown in many experiments and theoretical studies that two coupled chaotic systems can be synchronized in a sense that a chaotic system at the receiver can follow the time evolution of the identical system located in the transmitter. Therefore, a chaotic signal generated in the transmitter can be replicated in the receiver in a stable manner [14, 15]. The regime of the transmitter-receiver synchronization was proposed as a possible mechanism for the recovery of information encoded in the received chaotic signal [16–19].

A number of chaos-based covert communication methods that mix an information signal with a chaotic one and then recover the information using synchronization of chaos have been suggested [20]. In one class of these methods, the information signal  $m(t)$  is added to the chaotic output  $x_e(t)$  generated by a chaotic encoder whose oscillations do not depend on  $m(t)$ . The mixture  $x_e(t) + m(t)$  is transmitted to the decoder where it is used as a driving signal for the matched response system. Various implementations of the matched response systems were proposed; see, for example [1, 2, 21–24] and references therein. The common shortcoming of such methods of communication is that the driving signal which is “distorted” by the message  $m(t)$ , does not perfectly fit the decoder. As a result, the recovered message  $m_r(t)$  will always contain some traces of chaotic waveforms no matter how perfectly the parameters of the decoder match those of the encoder.

A different approach to the problem of chaotic encoding and decoding was suggested in a number of papers [3, 16–18, 25–27]. The main idea of this approach is that information signal  $m(t)$  is injected into one of the feedback loops of the chaotic system; see Figure 2.1. The feedback should be selected in such a way that the remaining subsystem (CT) is conditionally stable. In this case the distorted chaotic feedback signal  $x_e(t) + m(t)$  returns back to CT and drives the encoder oscillations. When the same signal,  $x_e(t) + m(t)$ , is applied to the decoder, it excites oscillations of the response system which are identical to the oscillations in the encoder. As the result the message  $m(t)$  can be recovered in the receiver using the open feedback loop of the response system. In this case (in the absence of noise), after initial transients, the information can be restored exactly.

All practical communication channels introduce signal distortions that alter the chaotic waveform, and as a result, the received chaotic oscillations do not precisely match the transmitter oscillations  $x_e(t) + m(t)$ . Channel noise, filtering, attenuation variability, and other distortions in the channel corrupt the chaotic carrier and information signal. The presence of these channel distortions significantly hamper the onset of identical synchronization of the chaotic systems [29, 30].

The strong sensitivity to the distortions of the chaotic signal and the resulting problems with chaos synchronization is the major obstacle for practical implementation of chaos-based communications systems. In order to overcome the problems of channel distortions, a number of special chaotic communication methods have been proposed [31–35]. At least in theory and nu-

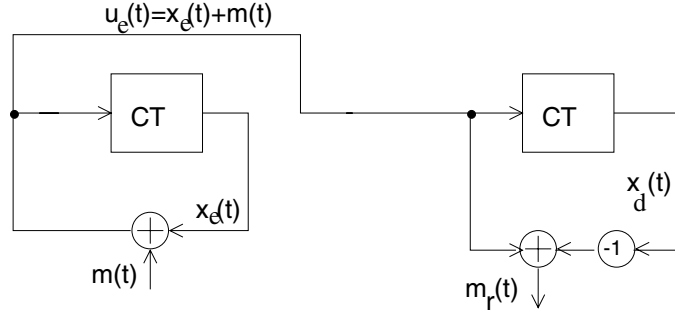


**Fig. 2.1.** Block-diagram of signal transmission with chaos suggested in [17]. (Reprinted with permission from [28], ©John Wiley & Sons, Ltd.)

merical simulations, it appears that the regime of identical synchronization in these specially designed systems is significantly less sensitive to channel noise and waveform distortions caused by the limited bandwidth of the channel [28, 36, 37].

One of the ways to minimize the effects of channel distortions was suggested in [38], where a chaotically timed pulse sequences substituted continuous chaotic waveforms. Each pulse in the sequence has identical shape, but the time delay between them varies chaotically. Because the information about the state of the chaotic system is contained entirely in the timing between pulses, the distortions that affect the pulse shape will not significantly influence the ability of the chaotic pulse generators to synchronize. Therefore synchronizing chaotic impulse generators can be utilized for communication via realistic wideband channels and at the same time allow the use of bandpass filters for noise reduction. The information can be encoded in the pulse train by alteration of time position of pulses with respect to chaotic carrier. This is the essence of the Chaotic Pulse Position Modulation (CPPM) system [39].

This proposed system belongs to the general class of ultra-wide bandwidth wireless communication systems. These systems received significant attention recently [40] (see also Chapter 4) because they offer a very promising alternative communication possibilities, especially in severe multipath environments or where they have to co-exist with a large number of other wireless systems. Chaotically varying spacing between narrow pulses enhances the spectral characteristics of the system by removing any periodicity from the transmitted signal. Because of the absence of characteristic frequencies, chaotically positioned pulses are difficult to observe and detect for the unauthorized user. Thus one expects that transmission based on chaotic pulse sequences can be designed to have a very low probability of intercept. A secure information transmission based on chaotic pulse trains with different methods of information encoding have been studied in [41].

The chapter is organized as follows. Section 2.2 gives a detailed overview of the CPPM system. In Section 2.3 we describe our implementation of the CPPM system and present the results of the experimental performance analysis in communication through a model channel with noise, filtering, and attenuation. We also consider the limitations in its performance caused by parameter mismatch between transmitter and receiver. The experimental setups we used for the analysis of CPPM performance in realistic noisy channels are described in Section 2.4. The channels we studied include a model bandlimited channel with white Gaussian noise, a low-power wireless link, and a free-space laser communication link. The last channel was characterized by the presence of severe communication signal distortions caused by atmospheric turbulence. Results of the experimental analysis are discussed in Section 2.5. Section 2.6 describes a modification of the CPPM which improves the performance of CPPM in multiuser environments.

## 2.2 CPPM Basics

In this section we describe the Chaotic Pulse Position Modulation system (CPPM). The CPPM method was suggested as a possible modification of the chaos-based communication approach shown in Figure 2.1 which significantly reduces the sensitivity of this communication to the channel distortions [39].

### 2.2.1 CPPM Principle and Operation

Consider a chaotic pulse generator that produces the chaotic pulse signal

$$U(t) = \sum_{j=0}^{\infty} w(t - t_j), \quad (2.1)$$

where  $w(t - t_j)$  represents the waveform of a pulse generated at time  $t_j = t_0 + \sum_{n=0}^j T_n$ , and  $T_n$  is the time interval between the  $n$ th and  $(n-1)$ th pulses. We assume that the sequence of the time intervals,  $T_i$ , represents iterations of a chaotic process. For simplicity we consider the case where chaos is produced by a one-dimensional map  $T_n = F(T_{n-1})$ , where  $F(\cdot)$  is a nonlinear function. Some studies of such chaotic pulse generators can be found in [38, 42].

The information is encoded within the chaotic pulse signal by using additional delays in the interpulse intervals,  $T_n$ . As a result, the generated pulse sequence is given by a new map

$$T_n = F(T_{n-1}) + d + mS_n, \quad (2.2)$$

where  $S_n$  is the information-bearing signal. Here we consider only the case of binary information, and therefore,  $S_n$  equals zero or one. The parameter  $m$  characterizes the amplitude of modulation. The parameter  $d$  is a constant

time delay which is needed for practical implementation of our modulation and demodulation method. The role of this parameter is discussed later. In the design of the chaotic pulse generator, the nonlinear function  $F(\cdot)$ , and parameters  $d$  and  $m$  are selected to guarantee chaotic behavior of the map.

The modulated chaotic pulse signal  $U(t) = \sum_{j=0}^{\infty} w(t - t_0 - \sum_{n=0}^j T_n)$ , where  $T_n$  is generated by Eq. (2.2), is the transmitted signal. The duration of each pulse  $w(t)$  in the pulse train is assumed to be much shorter than the minimal value of the interpulse intervals,  $T_n$ . To detect information at the receiver end, the decoder is triggered by the received pulses,  $U(t)$ . The consecutive time intervals  $T_{n-1}$  and  $T_n$  are measured and the information signal is recovered from the chaotic iterations  $T_n$  with the formula

$$S_n = (T_n - F(T_{n-1}) - d)/m. \quad (2.3)$$

If the nonlinear function,  $F(\cdot)$ , and parameters  $d$  and  $m$  in the receiver are the same as in the transmitter, then the encoded information  $S_n$  can be easily recovered. When the nonlinear functions are not matched with sufficient precision, a large decoding error results. Therefore, an unauthorized receiver who has no information about the dynamical system producing chaotic pulses in the transmitter cannot determine whether a particular received pulse was delayed with respect to its original (chaotic) position, and thus whether  $S_n$  was “0” or “1”.

Because the chaotic map of the decoder in the authorized receiver is matched to the map of the encoder in the corresponding transmitter, the time of the next arriving pulse can be predicted. In this case the input of the synchronized receiver can be blocked up to the moment of time when the next pulse is expected. The time intervals when the input to a particular receiver is blocked can be utilized by other users, thus providing a multiplexing strategy. Such selectivity based on the synchronization between the transmitter and the receiver can substantially improve the performance of the system by reducing the probability of false triggering of the decoder by channel noise.

The method described above is easy to implement in analog circuitry, and we used it in our experimental studies. However, we expect that various modifications of the detection method can be suggested to improve the system performance or simplify theoretical performance analysis. Consider one of them. When the demodulator is synchronized to the modulator, in order to decode a single bit of transmitted information the demodulator must simply determine whether a pulse from the transmitter was delayed relative to its anticipated position. If the ideal synchronization is established, but the signal is corrupted by noise, the optimal detection scheme operates as follows. Integrate the signal over the pulse duration inside the windows where pulses corresponding to “1” and “0” are expected to occur. The decision on whether “1” or “0” is received is made based upon whether the integral over “1”-window is larger or smaller than that over “0”-window. Such a detection scheme is employed in the ideal case of perfect synchronization in conventional (nonchaotic) Pulse Position Modulation (PPM) scheme. The performance of

this scheme is known to be 3 dB worse than the BPSK system. Although in the case of perfect synchronization this detection scheme is ideal, according to our numerical simulations, its performance quickly degrades when synchronization errors due to the channel noise are taken into account. For this reason and for the sake of design simplicity we use a threshold detector in all our experiments and analysis.

In a noise-free environment, the arrival time of chaotic pulses can be easily registered by a variety of methods. However, in a noisy environment, the receiver can mistake a large noise fluctuation for an incoming pulse, and detect the wrong information bit. Furthermore, this false pulse can destroy chaotic synchronization, and thus prompt a sequence of errors until the receiver re-synchronizes with the transmitter. In fact, one of the advantages of using chaotic pulse generators is that the system re-acquires synchronization automatically, without any specific “hand-shaking” protocol. The decoder only needs to detect two correct consecutive pulses in order to re-establish synchronization. We studied the bit-error performance in a noisy environment both theoretically and experimentally. The results of these studies are presented below.

### 2.2.2 CPPM BER Performance Evaluation

We characterize the performance of our system by studying the dependence of the bit-error rate on the ratio of energy per one transmitted bit to the spectral density of noise,  $E_b/N_0$ . This dependence is shown in Figure 2.3, where it is compared to the performance of more traditional communication schemes, BPSK, PPM, and noncoherent FSK.

We can obtain a rough analytical estimate of the CPPM BER performance of our detection scheme in the case of rectangular pulse shape. In order to do so, let us consider a simplified model of our detection method. In the detector the signal that is a sum of the transmitted pulse signal and WGN is low-pass filtered and is applied to a threshold element. Let us assume that the low-pass filter can be approximated by the running average filter:

$$y(t) = \frac{1}{\tau} \int_{t-\tau}^t x(\xi) d\xi.$$

Let the windows where the pulses corresponding to “1” and “0” have the same duration,  $T$ ; see Figure 2.2. We assume that the receiver maintains synchronization at all times, so that every “0”-pulse is within the “0”-window,  $0 < t \leq T$ , and every “1”-pulse is within the “1”-window,  $T < t \leq 2T$ . Let us divide the interval where “0”-pulse is expected into bins of duration  $1/f$ , where  $f$  is the filter cut-off frequency. We assume that  $f = 1/\tau$ ,  $\tau$  being the pulse duration, and that when a pulse arrives, it is contained entirely within one bin. We sample the output  $y(t)$  from the filter once at the end of every bin.

In our model detection scheme the threshold element is set off when the the output from one of the bins is larger than the threshold. If the threshold is crossed where a pulse corresponding to “0” is expected, a “0” is detected, otherwise a “1” is detected by default.

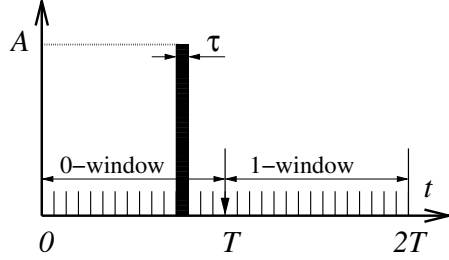


**Fig. 2.2.** The illustration of the detection scheme. (Reprinted with permission from [43], ©2001 IEEE.)

Let  $A$  be the pulse amplitude,  $H$ , the threshold value, and  $\sigma^2$ , the noise variance at the filter output.

First, we evaluate the error probability when “1” is transmitted,  $P_{0|1}$ . This probability can be found from  $P_{1|1} + P_{0|1} = 1$ , where  $P_{1|1}$ , the probability to correctly detect “1” can be easily found. It is the probability that the filter output,  $y_i$ , from any bin in the “0” does not exceed the threshold. Using the statistical independence of the measurements for each window in the case of white noise, we can write:

$$\begin{aligned} P_{1|1} &= \prod_{i=1}^{T/\tau} p_i(y_i < H) = [p(y < H)]^{T/\tau} = \left[ \frac{1}{\sqrt{2\pi\sigma^2}} \int_{-\infty}^H \exp\left(-\frac{x^2}{2\sigma^2}\right) dx \right]^{T/\tau} \\ &= \left[ \frac{1}{2} \left( 1 + \operatorname{erf}\left(\frac{H}{\sqrt{2\sigma^2}}\right) \right) \right]^{T/\tau} = \left[ \frac{1}{2} \left( 1 + \operatorname{erf}\left(h\sqrt{\frac{E_b}{N_0}}\right) \right) \right]^{T/\tau}. \end{aligned}$$

Here we introduced the relative threshold value,  $h = H/A$ , the energy per bit,  $E_b = A^2\tau$ , and the spectral power density of noise,  $N_0 = 2\sigma^2\tau$ .

The probability to detect “0” when “1” is transmitted is then:

$$P_{0|1} = 1 - P_{1|1} = 1 - \left[ \frac{1}{2} \left( 1 + \operatorname{erf}\left(h\sqrt{\frac{E_b}{N_0}}\right) \right) \right]^{T/\tau}.$$

The error probability in the case when “0” is transmitted can be found similarly. The error occurs when the output from all bins in the “0” window remains lower than the threshold, despite the fact that the transmitted signal is nonzero within one of them:

$$\begin{aligned}
P_{1|0} &= \left[ \frac{1}{\sqrt{2\pi\sigma^2}} \int_{-\infty}^H \exp\left(-\frac{x^2}{2\sigma^2}\right) dx \right]^{T/\tau-1} \\
&\quad \times \left[ \frac{1}{\sqrt{2\pi\sigma^2}} \int_{-\infty}^H \exp\left(-\frac{(x-A)^2}{2\sigma^2}\right) dx \right] \\
&= \left[ \frac{1}{2} \left( 1 + \operatorname{erf}\left(\frac{H}{\sqrt{2\sigma^2}}\right) \right) \right]^{T/\tau-1} \times \left[ \frac{1}{2} \left( 1 + \operatorname{erf}\left(\frac{H-A}{\sqrt{2\sigma^2}}\right) \right) \right].
\end{aligned}$$

Rewriting the last part of the equation in terms of the relative threshold value  $h$ , the energy per bit  $E_b$ , and the spectral power density of noise  $N_0$  one obtains

$$P_{1|0} = \left[ \frac{1}{2} \left( 1 + \operatorname{erf}\left(h\sqrt{\frac{E_b}{N_0}}\right) \right) \right]^{T/\tau-1} \times \left[ \frac{1}{2} \operatorname{erfc}\left((1-h)\sqrt{\frac{E_b}{N_0}}\right) \right].$$

The overall error probability is the combination of  $P_{1|0}$  and  $P_{0|1}$ :  $BER = p_1 P_{0|1} + (1 - p_1) P_{1|0}$  where  $p_1$  is the characteristic of the data stream which is the ratio of “1”s in it. In our experiment both  $p_1$  and  $h$  were equal to 1/2. In this case the expression for the BER can be written in a shorter form:

$$BER = \frac{1}{2} \left( 1 - \operatorname{erf}\left(\frac{\sqrt{\epsilon}}{2}\right) \left( \frac{1}{2} \left( 1 + \operatorname{erf}\left(\frac{\sqrt{\epsilon}}{2}\right) \right) \right)^{T/\tau-1} \right),$$

where  $\epsilon = E_b/N_0$

Figure 2.3 shows the BER performance of the CPPM as estimated analytically, computed in numerical simulations with  $h = 0.5$ ,  $p_1 = 0.5$ , and  $T/\tau = 10$  and measured in the experiment. The difference of approximately 1 dB between the analytical and numerical curves can be largely attributed to burst errors arising from the loss of synchronization, which is not taken into account in our model. Details on the experimental setup used to obtain the experimental BER data are given in Section 2.4.

## 2.3 CPPM implementation

### 2.3.1 CPPM Implementation

The implementation of the chaotic pulse modulator used in our experiments is illustrated in Figure 2.4. The Integrator produces a linearly increasing voltage,  $V(t) = \beta^{-1}(t - t_n)$ , at its output. At the Comparator this voltage is compared with the threshold voltage produced at the output of the nonlinear converter  $F(x)$ . The threshold level  $F(V_n)$  is formed by a nonlinear conversion of voltage  $V_n = V(t_n)$  which was acquired and saved from the previous iteration using sample and hold (S&H) circuits. When voltage  $V(t)$  reaches this threshold



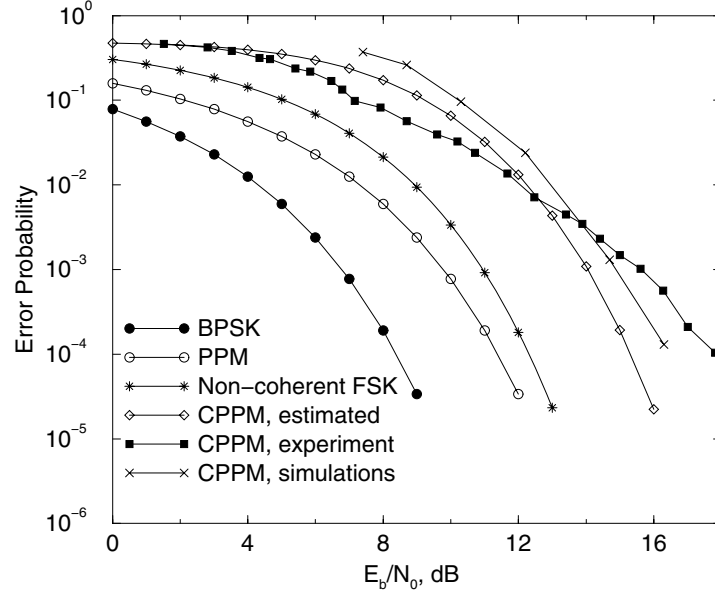


**Fig. 2.3.** Error probabilities of ideal BPSK, noncoherent FSK, and ideal PPM systems compared to the performance of the CPPM system. (Reprinted with permission from [43], ©2001 IEEE.)

level, the comparator triggers the Pulse Generator I. It happens at the moment of time  $t'_{n+1} = t_n + \beta F(V_n)$ . The generated pulse (Chaotic Clock Signal) causes the Data Generator to update the transmitted information bit. Depending on the information bit transmitted,  $S_{n+1}$ , the Delay Modulator delays the pulse produced by the Pulse Generator by the time  $d + mS_{n+1}$ . Therefore the delayed pulse is generated at the moment of time  $t_{n+1} = t_n + \beta F(V_n) + d + mS_{n+1}$ . Through the sample and hold circuit this pulse first resets the threshold to the new iteration value of the chaotic map  $V(t_{n+1}) \rightarrow F(V(t_{n+1}))$ , and then resets the integrator output to zero,  $V(t) = 0$ . The dynamics of the threshold value is determined by the shape nonlinear function  $F(\cdot)$ . The spacing between the  $n$ th and  $(n+1)$ th pulses is proportional to the threshold value  $V_n$ , which is generated according to the map

$$T_{n+1} = \beta F(\beta^{-1}T_n) + d + mS_{n+1}, \quad (2.4)$$

where  $T_n = t_{n-1} - t_n$ , and  $S_n$  is the binary information signal. In the experimental setup the shape of the nonlinear function was built to have the following form

$$F(x) \equiv \alpha f(x) = \begin{cases} \alpha x & \text{if } x < 5V, \\ \alpha(10V - x) & \text{if } x \geq 5V. \end{cases} \quad (2.5)$$

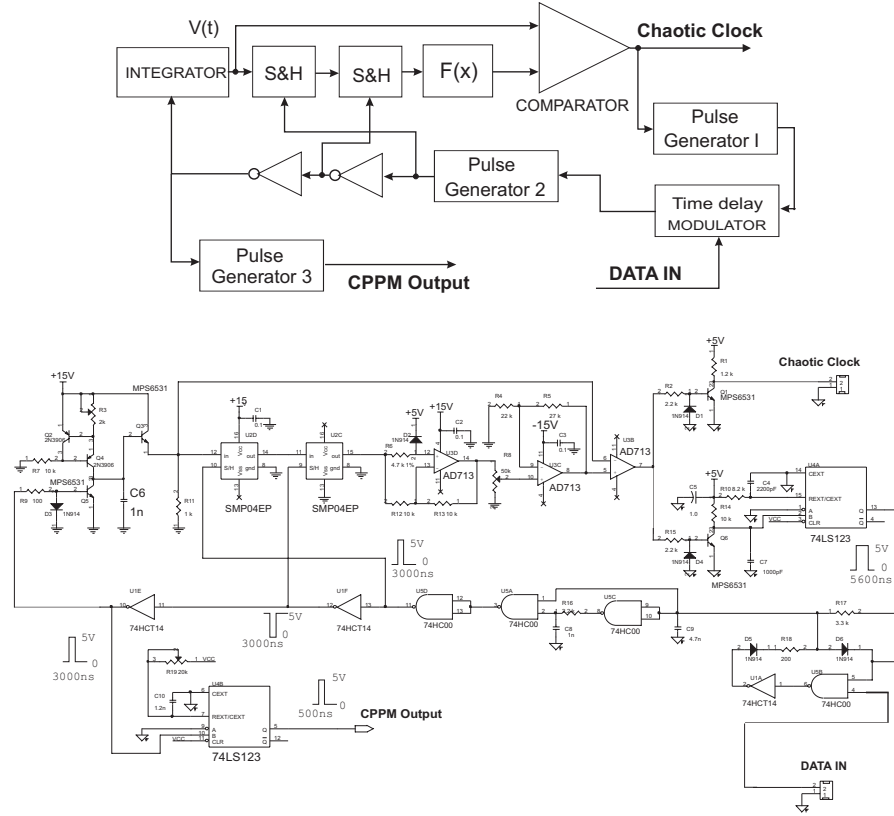


**Fig. 2.4.** Block diagram (top panel) and schematics (bottom panel) of the chaotic pulse modulator.

The selection of the nonlinearity in the form of a piecewise linear function helps to ensure the robust regimes of chaos generation for rather broad ranges of parameters of the chaotic pulse position modulator.

The position-modulated pulses,  $w(t - t_j)$ , are shaped in the Pulse Generator II. These pulses form the output signal  $U(t) = \sum_{j=0}^{\infty} w(t - t_j)$ , which is transmitted to the receiver.

The demodulator scheme is illustrated in Figure 2.5. In the receiver the Integrator, S&H circuits, and the nonlinearity block generating the threshold values are reset or triggered by the pulse received from the transmitter rather than by the pulse from the internal feedback loop. To be more precise, they are triggered when the input signal,  $U(t)$ , from the channel exceeds a certain input threshold. The time difference between the anticipated location of the pulse without modulation,  $t'_{n+1} = t_n + \beta F(V_n)$ , and the actual arrival time  $t_{n+1}$  translates into the difference between the threshold value,

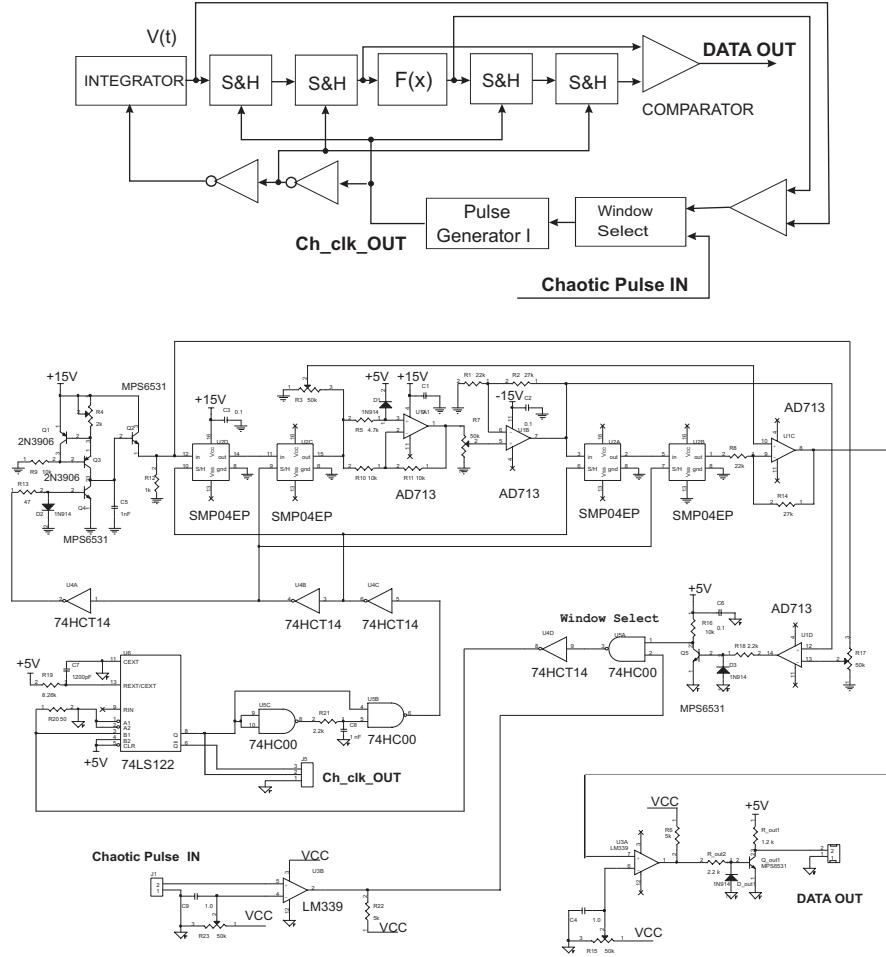


**Fig. 2.5.** Block diagram (top panel) and schematics (bottom panel) of the chaotic pulse demodulator.

$F(V_n)$  generated by the nonlinear function and the voltage,  $V(t_{n+1})$  at the Integrator at the moment when the input signal  $U(t)$  exceeds the input threshold. For each received pulse the difference  $V(t_{n+1}) - F(V_n)$  is computed and is used for deciding whether the pulse was delayed. If this difference is less than the reference value  $\beta(d + m/2)$ , the detected data bit  $S_{n+1}$  is “0”; otherwise it is “1”.

Another important part of the receiver is the Window Selection block. Once the receiver correctly observes two consecutive pulses, it can predict the earliest moment of time when it can expect to receive the next pulse. This means that we can block the input to the demodulator circuit until shortly

before such a moment. This is done by the Window Select block. In the experiment, this circuit opens the receiver input at the time  $t'_{n+1} = t_n + \beta F(V_n)$  by Window Control pulses generated by the Comparator (see Figure 2.5). The input stays open until the decoder is triggered by the first pulse received. Using such windowing greatly reduces the chance of the receiver being triggered by noise, interference, or pulses belonging to other users, however, it may increase the time necessary to re-acquire synchronization after a string of erroneous pulses.

### 2.3.2 Parameters Mismatch Limitations

It is known that because the synchronization-based chaotic communication schemes rely on the identity of synchronous chaotic oscillations, they are susceptible to negative effects of parameter mismatches. Here we evaluate how precisely the parameters of our modulator and demodulator have to be tuned in order to ensure errorless communication over a distortion-free channel.

The information detection in our case is based on the measurements of time delays, therefore it is important that the modulator and the demodulator can maintain synchronous time reference points. The reference point in the modulator is the front edge of the chaotic clock pulse. The reference point in the demodulator is the front edge of the window control pulse. Ideally, if the parameters of the modulator and the demodulator were exactly the same and the systems were synchronized, then both reference points would be always at the times  $t'_{n+1} = t_n + \beta F(V_n)$ , and the received pulse would be delayed by the time  $d$  for  $S_{n+1} = 0$  and  $d + m$  for  $S_{n+1} = 1$ . In this case, setting the bit separator at the delay  $d + m/2$  would guarantee errorless detection in a noise-free environment.

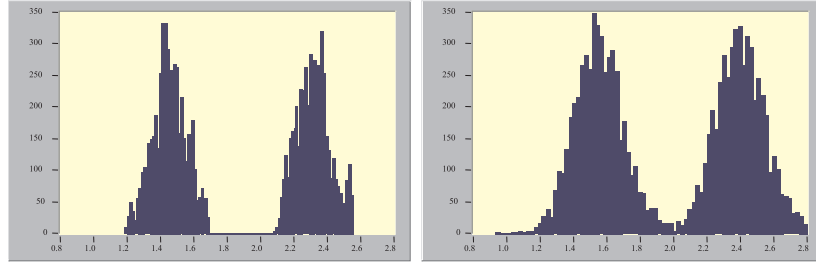


**Fig. 2.6.** Histograms of the fluctuations of the received pulse positions with respect to the receiver reference point: noise-free channel (left) and channel with WGN  $E_b/N_o \sim 18$  dB (right). (Reprinted with permission from [43], ©2001 IEEE.)

In an analog implementation of a chaotic pulse position modulator and demodulator system, the parameters of the circuits are never exactly the same.

Therefore, the time positions  $t_n^{(M)}$  and  $t_n^{(D)}$  of the reference points in the modulator and the demodulator chaotically fluctuate with respect to each other. Due to these fluctuations the position of the received pulse,  $t_n = t_n^{(M)} + d + S_n$ , is shifted from the arrival time predicted in the demodulator,  $t_n^{(D)} + d + S_n$ . The errors are caused by the following two factors. First, when the amplitude of fluctuations of the position shift is larger than  $m/2$ , some delays for “0”s and “1”s overlap and cannot be separated. Second, when the fluctuations are such that a pulse arrives before the demodulator opens the receiver input ( $t_n < t_n^{(D)}$ ), the demodulator skips the pulse, loses synchronization and cannot recover the information until it resynchronizes. In our experimental setup the parameters  $\beta_{M,D}$  were tuned to be as close as possible, and the nonlinear converters were built using 1% components. The fluctuations of the positions of the received pulses with respect to the window control pulse were studied experimentally by measuring time delay histograms. Figure 2.6 presents typical histograms measured for the case of a noise-free channel and for a channel with noise when  $E_b/N_o \sim 18$  dB.

Assuming that systems were synchronized up to the  $(n - 1)$  pulse in the train, the fluctuations of the separation between the reference time positions equal

$$\Delta_n \equiv t_n^{(D)} - t_n^{(M)} = \beta_D F_D(\beta_D^{-1} T_{n-1}) - \beta_M F_M(\beta_M^{-1} T_{n-1}), \quad (2.6)$$

where indices  $D$  and  $M$  stand for demodulator and modulator, respectively. As discussed above, in order to achieve errorless detection, two conditions should be satisfied for all time intervals in the chaotic pulse train produced by the modulator. These conditions are the synchronization condition,  $\{\Delta_n\}_{\max} < d$ , and the detection condition  $\{|\Delta_n|\}_{\max} < m/2$ . As an example we consider the simplest case where all parameters of the systems are the same except for the mismatch of the parameter  $\alpha$  in the nonlinear function converter; see Eq. (2.5). Using Eq. (2.5) and Eq. (2.6) the expression for the separation time can be rewritten in the form

$$\Delta_n = (\alpha_D - \alpha_M) \beta f(\beta^{-1} T_{n-1}). \quad (2.7)$$

It is easy to show that the largest possible value of the nonlinearity output  $f(\cdot)$ , which can appear in the chaotic iterations of the map, equals 5 V. Note that in the chaotic regime only positive values of  $f(\cdot)$  are realized. Therefore, if conditions

$$\beta(\alpha_D - \alpha_M) < d/5V \quad \text{and} \quad 2\beta|\alpha_D - \alpha_M| < m/5V. \quad (2.8)$$

are satisfied and there is no noise in the channel, then information can be recovered from the chaotic pulse train without errors.

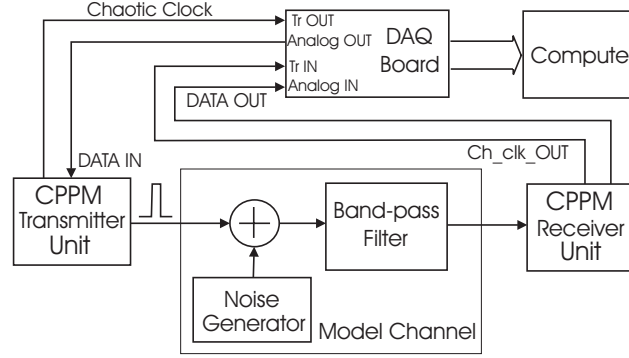


**Fig. 2.7.** Diagram of the experiment.

## 2.4 Experimental Studies of CPPM with Channel Distortions

### 2.4.1 CPPM Experiment with Model Channel

For the experimental evaluation of BER performance in a bandlimited noisy channel we transmitted the CPPM signal mixed with white Gaussian noise over a channel modeled with an active bandpass filter (Figure 2.7). We used a computer with a data acquisition board as the data source. Each update of the information bit loaded to the CPPM encoder was triggered by the chaotic clock generated in the transmitter. The computer calculated the displacement of the received chaotic pulse from the demodulator subtractor and detected the received information bit using a threshold element.

The model channel circuit consisted of a WGN generator and a bandpass filter with the pass band 1 kHz-500 kHz. The pulse duration was 500 ns. The distance between the pulses varied chaotically between 12  $\mu$ s and 25  $\mu$ s. This chaotic pulse train carried the information flow with the average bit rate  $\sim 60$  kb/sec. The amplitude of pulse position modulation  $m$  was 2  $\mu$ s. More details on the spectral characteristics of CPPM signals in passing through this model channel can be found elsewhere [43].

### 2.4.2 Wireless Implementation of CPPM

We have implemented and tested a low-power prototype of a wireless digital communication link using the chaotic pulse modulator and demodulator described above. The circuit diagrams of the transmitter and receiver units, which were added to the CPPM modulator and demodulator blocks to provide the wireless link, are shown in Figures 2.8 through 2.11.

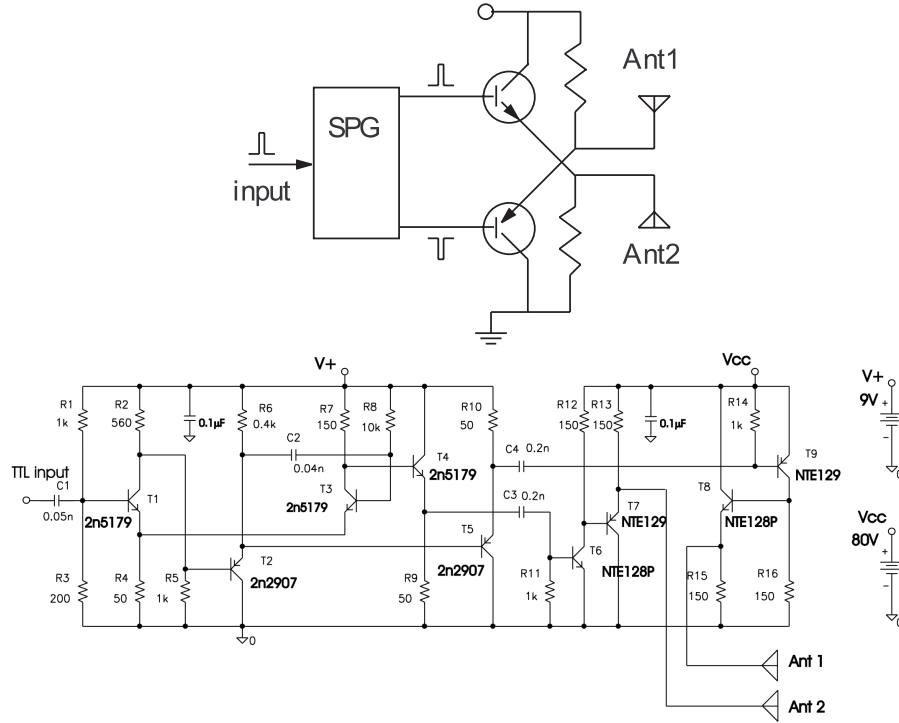


**Fig. 2.8.** Block-diagram (top panel) and schematics (bottom panel) of the ultra-wideband transmitter used in the wireless CPPM communication system.

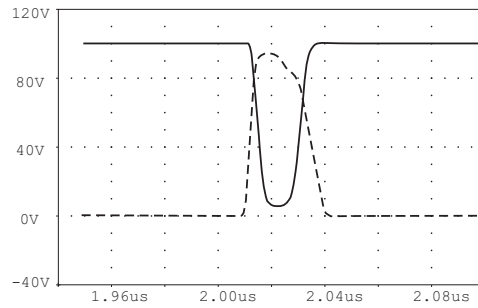


**Fig. 2.9.** Voltage pulse on the transmitter antennas Ant1 (solid line) and Ant2 (dotted line) in the exciter circuit, shown in Figure 2.8 with  $V_{cc} = 100$  V. Plots are calculated using a MicroSim circuit simulator.

## Transmitter

The transmitter contains the generator of a pair of symmetric short pulses (SPG) and the symmetric exciter for the two-pole antenna; see Figure 2.8. SPG is triggered by a TTL pulse (500 ns) from the output of the CPPM modulator (see Figure 2.4) and generates a short pulse (20 ns measured at a half of the amplitude). This short pulse is applied to the symmetric exciter that has two outputs; see Figure 2.9. The first output produces a high voltage positive pulse. The second output produces a high voltage negative pulse. These two outputs are applied to the corresponding poles of the antenna.

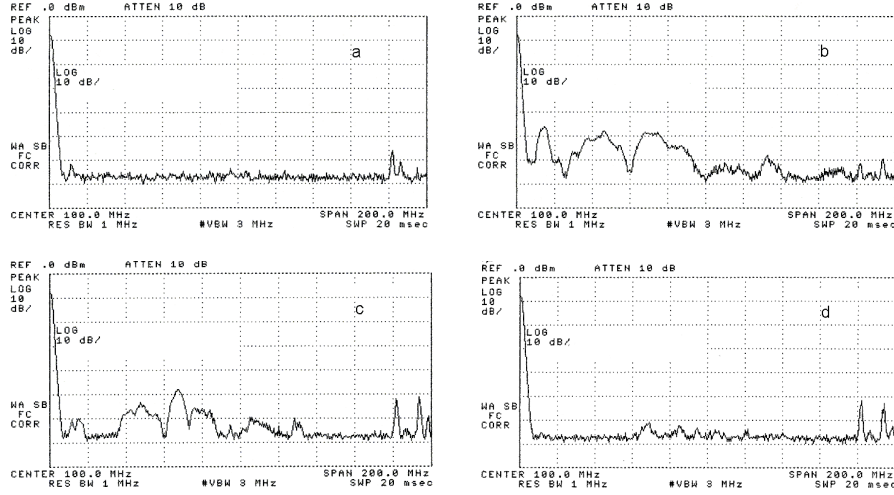


**Fig. 2.10.** Power spectral density of signals measured in the frequency range from 0 to 200 MHz. The background noise measured with the CPPM transmitter turned off is shown in (a). Panels (b), (c), and (d) present the spectra of the CPPM signal measured at the distance  $L$  from the CPPM transmitting antenna:  $L = 1$  m (b);  $L = 3$  m (c) and  $L = 10$  m (d). (Reprinted with permission from [43], ©2001 IEEE.)

## Receiver

The block diagram of the receiver is presented in Figure 2.11. The electromagnetic pulses received by the two-pole antenna (Ant1 and Ant2) are applied to the differential amplifier whose output is then amplified in the two-stage amplifier (Amp) and sent to the symmetric detector circuit. The output of the symmetric detector is then amplified by the second differential amplifier to generate enough voltage for triggering the pulse generator (PG) which produces the TTL pulse of the duration about 500 ns. The TTL pulse is then applied to the CPPM demodulator block shown in Figure 2.5.



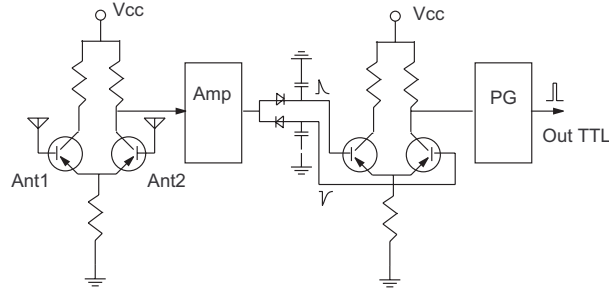


**Fig. 2.11.** Block diagram of the pulse receiver. (Reprinted with permission from [43], ©2001 IEEE .)

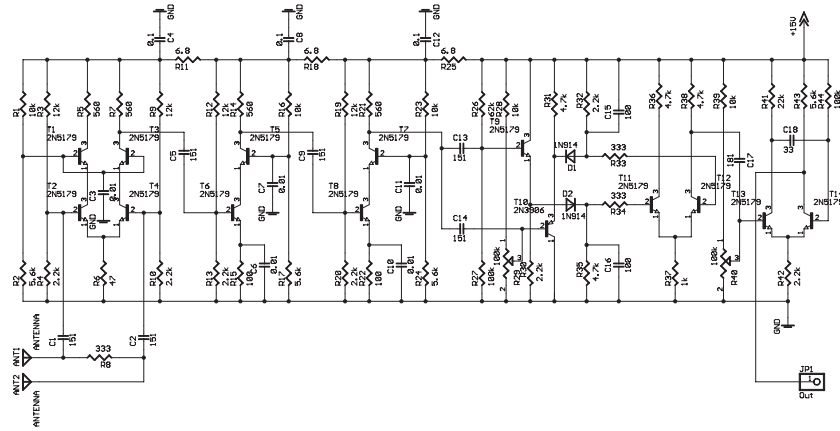


**Fig. 2.12.** Schematics of the ultra-wideband receiver used in the wireless CPPM system.

We tested our prototype wireless CPPM system in indoor experiments with separation between transmitter and receiver of up to 15 m and were able to achieve a stable regime of error-free communication.

### 2.4.3 Optical Chaos Communication Through Turbulent Atmosphere

The ability of the self-synchronizing CPPM method to communicate in the presence of significant nonstationary signal distortions in the channel has been studied experimentally using a free-space laser communication link [44]. Here the communication carrier signal consists of a sequence of optical pulses that travel through air. The characteristics of the communication channel are thus

determined by the optical properties of air and the severe communication signal distortions in this experiment are a result of atmospheric turbulence.

A schematic representation of the chaotic free-space laser communication system is shown in Figure 2.13. In this experiment the CPPM modulator circuit described in Section 2.3.1 was used to modulate the output-intensity of a semiconductor laser ( $\lambda = 690$  nm). The resulting intensity-modulated 10 mW semiconductor laser beam was coupled into a single-mode fiber. The beam emanating from the fiber was first expanded to a 4 in. diameter using a lens relay system (lenses  $L_1, L_2$ ) and a Celestron transmitter-telescope and was then directed through a 26 ft long vertical air-locked pipe to a  $45^\circ$  mirror placed inside a shed on the roof of the building. From there the light propagated over an atmospheric path of length  $L \simeq 2.5$  km to a 4 in. corner cube reflector placed on top of a water tower. After reflection the laser beam propagated from the water tower back to a communication receiver telescope on the roof-mounted shed. The receiver system used the same Celestron telescope and lens relay system (lenses  $L_1$  and  $L_3$ ) as did the transmitter system. The total double-pass atmospheric laser beam propagation distance was approximately  $2L \simeq 5$  km long. The received light power was registered by the PIN photo-detector (PDA55) placed in the lens  $L_3$  focal plane, amplified by the low-noise preamplifier (SR560 with a gain of 20), and the resulting signal served as input to the CPPM demodulator circuit (see Section 2.3.1).

## 2.5 CPPM Performance and Features

### 2.5.1 Experimental BER Performance Evaluation

We experimentally evaluated the BER performance of CPPM system using the model channel setup shown in Figure 2.7. We measured the dependence of BER on the ratio  $E_b/N_0$ , where  $E_b$  is the energy of CPPM signal per bit and  $N_0$  is the spectral density of noise. This dependence is plotted in Figure 2.3 along with the analytical and numerical estimates that we discussed in Section 2.2.

The slightly better than expected performance of the experimental system at high levels of noise can be explained by the observed significant deviations of the noise distribution from Gaussian at high noise amplitudes. The quicker than expected degradation of performance at low levels of noise is primarily due to the small mismatch of the parameters in the transmitter and the receiver. Still, considering the crudeness of the analytical model and the experimental difficulties, all three plots agree reasonably well.

### 2.5.2 Effects of Atmospheric Turbulence in an Optical Chaos Communication Experiment

We tested the self-synchronizing CPPM communication scheme in an experiment where information was transmitted over a  $\sim 5$  km laser link through

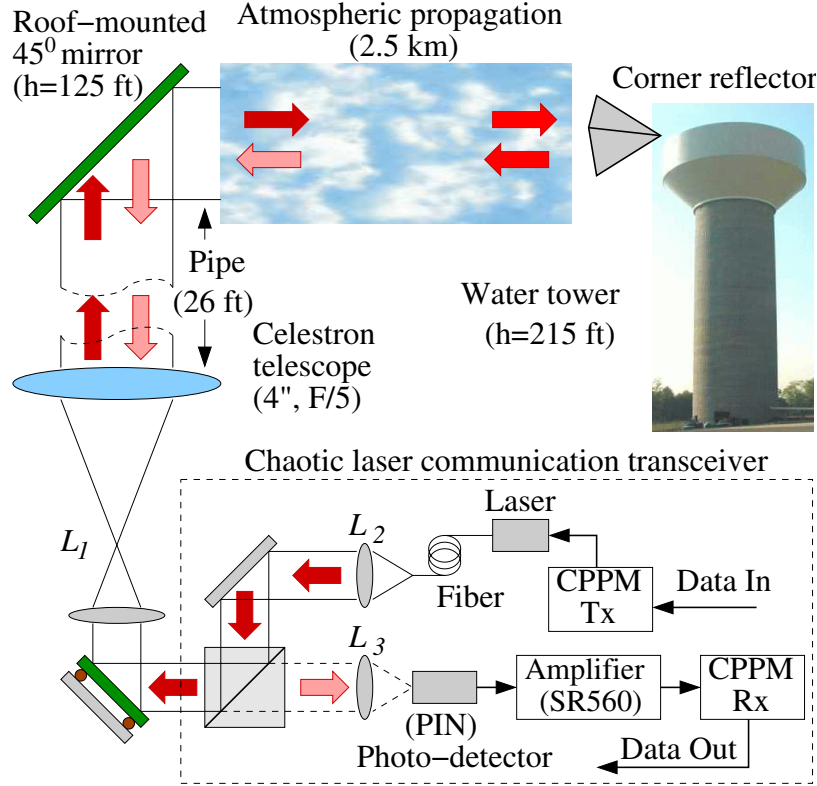


**Fig. 2.13.** Schematic for the free-space laser communication system based on the CPPM transceiver. Details are given in the text. (Reprinted with permission from [44], ©2002 American Physical Society.)

turbulent air. Turbulence in the atmospheric communication channel leads to severe laser beam intensity scintillations that result in deep fluctuations of the received communication signal (received laser beam power). The most deleterious effects from receiver plane scintillations are the loss of signal-to-noise ratio and drop-outs (information loss).

To demonstrate the level of intensity scintillations in the atmospheric channel, we measured the received signal from a continuously running laser with constant output intensity. Figure 2.14a shows the fluctuations of the normalized received power, measured by the PIN photodetector placed in the lens  $L_3$  focal plane (Figure 2.13), amplified by the low noise preamplifier (SR500 with gain of 20), and then acquired with sampling rate 1000 samples/sec. The corresponding ensemble-averaged received signal power spectrum  $S(f)$  is shown in Figure 2.14b. The severeness of the signal distortions is clearly visible in Figure 2.14 and is quantified by an estimated standard deviation of the normalized received signal as high as 0.8-0.9, which is indicative of a

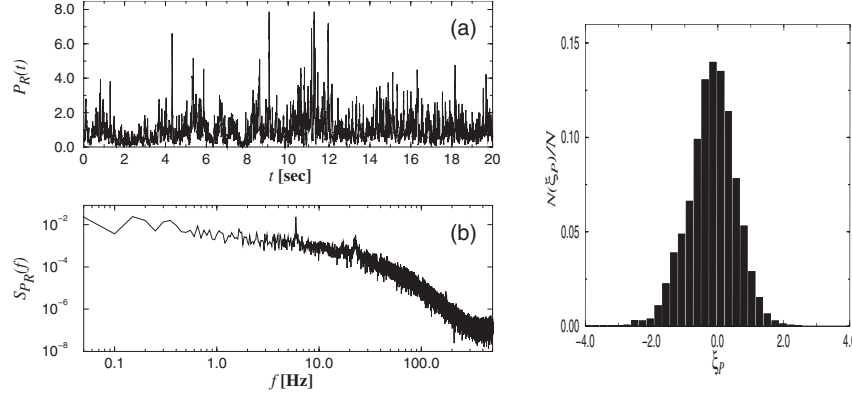


**Fig. 2.14.** Fluctuations of the received power  $P(t)$  in the experiment with a non-modulated laser generating a constant output intensity (10 mW). The normalized received power  $P(t)/\langle P(t) \rangle$  measured at the photo-detector output (a), and the corresponding averaged power spectrum (b) illustrate the presence of strong laser beam intensity scintillations. (c) Histogram of the probability distribution for the random variable  $\ln(P/\langle P \rangle)$ . (Reprinted with permission from [44], ©2002 American Physical Society.)

strong scintillation regime. In atmospheric optics the laser beam scintillations are traditionally described in terms of the distribution of the logarithm of the received power (for finite receiver telescope):  $\ln(P/\langle P \rangle)$ , where  $\langle P \rangle$  is the ensemble (time) averaged value [45]. The histogram of the random variable  $\ln(P/\langle P \rangle)$  is shown in Figure 2.14c. Representing an approximation to the probability distribution of the received power the histogram closely matches the log-normal distribution that theory predicts for turbulent atmosphere [45].

In the communication experiment the CPPM modulator described in Section 2.3.1 (denoted by CPPM Tx in Figure 2.13) generates a sequence of TTL pulse signals that are used to trigger the laser resulting in a chaotic sequence of short-term ( $\sim 1.0 \mu\text{s}$ ) pulses of light intensity. The interpulse intervals  $\{T_n\}$  fluctuated chaotically ranging from  $10 \mu\text{sec}$  to  $25 \mu\text{sec}$  and supported a  $\sim 60$  kbit per sec bit-rate. After the double-pass propagation through air the distorted light pulses are detected by the PIN photo diode, the output of which is applied to the CPPM demodulator circuit (CPPM Rx in Figure 2.13). If the output exceeds a certain input threshold, which in our experiment was set to  $\sim 200$  mV, the timer circuit in CPPM Rx is triggered and the information signal is recovered from the chaotic iterations of interpulse intervals,  $\{T_n\}$ , using formula (2.3).

The CPPM communication method encodes information in the interpulse intervals  $\{T_n\}$  and can therefore tolerate strong signal distortions and amplitude variations like the ones caused by atmospheric turbulence as long as fluctuations of the propagation time in the turbulent channel remain small. Figure 2.15a illustrates the severe pulse amplitude fluctuations of the signal

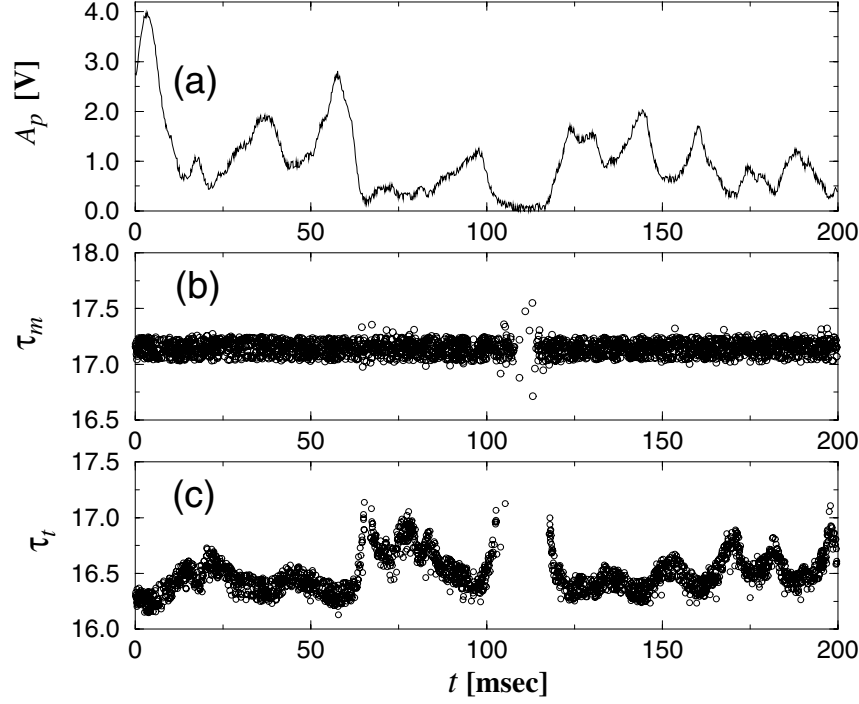


**Fig. 2.15.** Fluctuations of the CPPM pulses of light intensity after traveling through atmospheric turbulence. Pulse amplitude  $A_p$  measured in volts at the output of amplifier (a). Propagation times  $\tau_m$  (b) and  $\tau_t$  (c) in  $\mu\text{sec}$ . The pulse propagation times are computed from data acquired simultaneously at the output of CPPM Tx and output of Amplifier (SR560) at a sampling rate of  $5 \times 10^6$  samples per sec. (Reprinted with permission from [44], ©2002 American Physical Society.)

entering the CPPM demodulator. Figure 2.15b shows the pulse propagation time  $\tau_m$ , which is measured between the leading front of the TTL pulse applied to the laser and the maximal point of the received pulse. It varied only within a  $0.2 \mu\text{sec}$  time interval. However, in order to trigger CPPM Rx the received pulse amplitude has to exceed a certain threshold level. This level ( $\sim 200 \text{ mV}$ ) was selected to minimize instances of receiver controller triggering caused by noise, or by pulses originating from local pulse reflections off nearby optical surfaces. Therefore, the actual delay time  $\tau_t$ , measured between the leading front of TTL pulses generated by CPPM Tx and the moments of CPPM Rx triggering, depends on the amplitude of the received pulses and fluctuates; see Figure 2.15c. Although  $\tau_t$  changes with the amplitude variation these changes remain less than the modulation amplitude  $m \sim 1.5 \mu\text{sec}$ ; see Eq. (2.2). Thus, the variations of the pulse propagation time are small enough

for the CPPM controller to self-synchronize and to maintain the stability of the communication link.

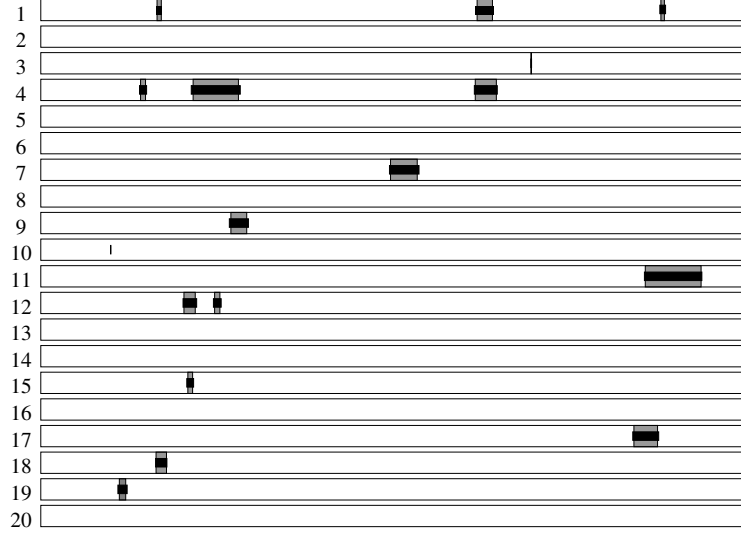


**Fig. 2.16.** Typical structure of errors shown in 20 consecutive measured data streams each of length  $\sim 170$  msec transmitted at  $\sim 2$  min intervals. Each strip presents 10,000 bits which are transmitted with the CPPM method. White intervals of the strips mark blocks of data received without errors. Narrow black ribbons in the middle of strips mark the blocks of the data received with errors. The gray background shows the blocks of the dropped-out data caused by the loss of CPPM pulses due to fading instances.

The gaps visible in Figures 2.15b and 2.15c are caused by pulse amplitude fading when the pulse amplitude falls to the photo-receiver noise level and below threshold level, respectively. The gaps are audible as occasional clicks, when using the free-space laser communication system described here for real-time voice communication, which was implemented by digitizing the output of a microphone with a delta-modulator and transmitting the binary signal. Except for these short-term (less than 50 msec) drop-offs, the voice communication was stable and clear.

Figure 2.16 shows an example of a map of communication errors that resulted from the transmission of binary pseudo-random data. The total BER of  $1.92 \times 10^{-2}$  measured in this experiment has three contributions. First, the loss of bits carried by the pulses that did not trigger the CPPM receiver due to the fading in the channel contributes  $\sim 1.78 \times 10^{-2}$  to the BER ( $\sim 92.7\%$ ). The fading moments occur randomly during the communication and cause the drop-outs of blocks of data up to 1000 consecutive bits. Second, errors

that occur within time intervals immediately before and after the failure of communication by fading contribute  $\sim 1.4 \times 10^{-3}$  to the BER ( $\sim 7.3\%$ ). In these time intervals the amplitude of the received pulses is still close to the threshold and, as a consequence, even small noise in the channel can result in significant fluctuation of the interpulse intervals (see Figure 2.15c). Third, errors that are not related to the complete failure of the channel because of fading instances contributed to the BER only  $\sim 5.5 \times 10^{-5}$ .

This structure of errors indicates that the CPPM communication method supports robust communication over a turbulent channel except for instances when the communication link fails due to fading. Thanks to the self-synchronizing feature of the CPPM method and the fact that the CPPM receiver needs to obtain just two consecutive correct pulses to re-establish the regime of chaos synchronization, the communication after drop-out events is re-established almost immediately.

### 2.5.3 Wireless CPPM and Low Probability of Detection

In the experiments with wireless CPPM, we studied spectral characteristics of the chaotic pulse signal radiated by the wireless CPPM. The Power Spectral Density (PSD) was measured with HP 8590A Portable RF Spectrum Analyzer using a two-pole receiving antenna. The results of the measurements are presented in Figure 2.10. The PSD of the signal received by the RF spectrum analyzer, when the CPPM transmitter is turned off, is shown in Figure 2.10a. The spectrum was measured in the range of frequencies from 1 MHz to 200 MHz with the video bandwidth filter of 3 MHz. The same measurements were done when the CPPM transmitter was turned on. The amplitude of the pulse measured across the poles of the transmitting antenna is about 130 V. Duration of the pulse is about 30 nsec. Figure 2.10 presents measured PSD of the received RF signal at two distances from the transmitting antenna (1 and 10 m). As one can see, already at 10 m the signal PSD is at the level or below the background RF noise. This shows a potential for using CPPM systems in applications requiring low probability of detection.

Here we use the results of the experimental analysis of radiated pulse signals to illustrate the advantages of CPPM over more conventional communications schemes in the area of low probability of detection. The existing communications schemes rely on digitally generated pseudo-random sequences to eliminate from transmitted signals the features that allow an adversary to detect and intercept the transmission. This approach has two intrinsic shortcomings.

First, the pseudo-random sequences eventually repeat, and second, the digital character of the generation algorithm introduces into the signal features associated with the corresponding quantization. These two points are illustrated in Figure 2.17, where we show the spectrum of a pseudo-random pulse sequence transmitted by the same method as in the CPPM transmission. The transmitted signal consisted of a periodically repeated sequence of 128 pulses

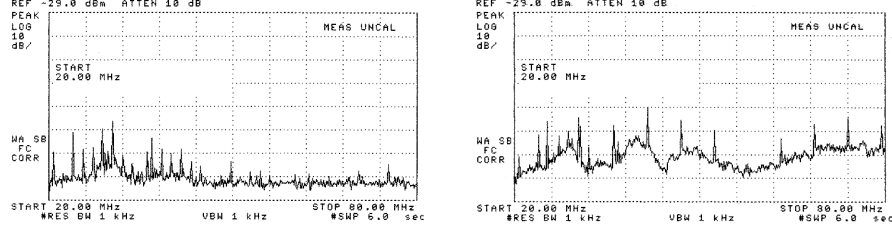


**Fig. 2.17.** The spectrum of a transmission of a pulse train with pseudo-random pulse timing (left panel). The reference spectrum of the background (right panel). The start frequency is 20 MHz and the stop frequency is 80 MHz. (Reprinted with permission from [43], ©2001 IEEE.)

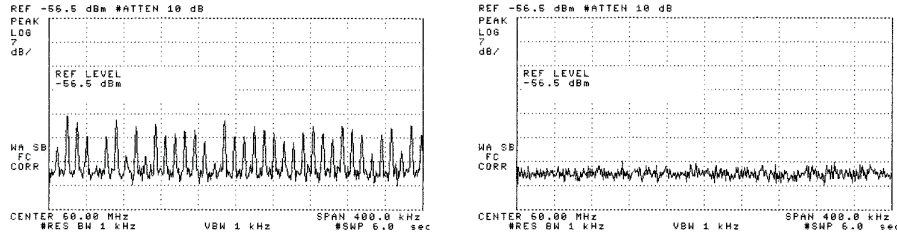


**Fig. 2.18.** The spectrum of a transmission of a pulse train with pseudo-random pulse timing (the same as in Figure 2.17), but measured at a finer frequency resolution (left panel). A typical spectrum of a CPM transmission measured with the same resolution (right panel). (Reprinted with permission from [43], ©2001 IEEE.)

with the timing determined by the raising edges of a pseudo-random sequence of the length of 511 bits.

In Figure 2.17 (left panel) one can clearly see the periodicity due to the quantization in the pseudo-random timing sequence, with the chip rate  $\sim 5.4$  MHz. The peaks in Figure 2.18 (left panel) are due to the periodic repetition of the pseudo-random sequence, with the characteristic frequency  $\sim 10.5$  kHz. Either of these features can be exploited in order to detect such transmission. For comparison, in Figure 2.18 (right panel) we see the spectrum of a chaotic pulse train, with the same frequency resolution as in Figure 2.18 (left panel). CPM avoids both sources of periodicity present in the pseudo-random pulse train transmission, and, as expected, its spectrum does not show the corresponding peaks.

More complicated methods<sup>1</sup> used for detection of pseudo-random pulse transmissions can be applied in order to discover chaotic pulse transmission.

<sup>1</sup> We should point out that such simple and apparent scheme as observing a pulse sequence on an oscilloscope is not very efficient in a noisy environment, with band-pass filtering due to antennas. Many (or all, if there is no transmission) pulses will appear due to noise.



These methods, however, become much more efficient if one can recover a time reference, which in the case of CPPM transmission is more difficult.

## 2.6 Multiuser Extension of CPPM

Direct application of CPPM in a multiuser environment leads to a significant performance degradation. If multiple transmitters are operating at the same time, receiver “A” can capture pulses from other transmitters which would occasionally fit into the reception windows of the receiver, thus creating errors in the bit detection, and moreover, causing synchronization breakdowns. To reduce the probability of these events, we propose to send a fixed group of pulses instead of a single pulse. The structure of the pulse train should be unique for a given user, and the transmission time for the train as before is determined by the chaotic map. The detection of the pulse train arrival is achieved by the matched filter (correlation detector), thus providing selectivity and processing gain. The output of the correlator is then processed in the receiver in the same way as a single pulse is processed in the original scheme shown in Figure 2.5.

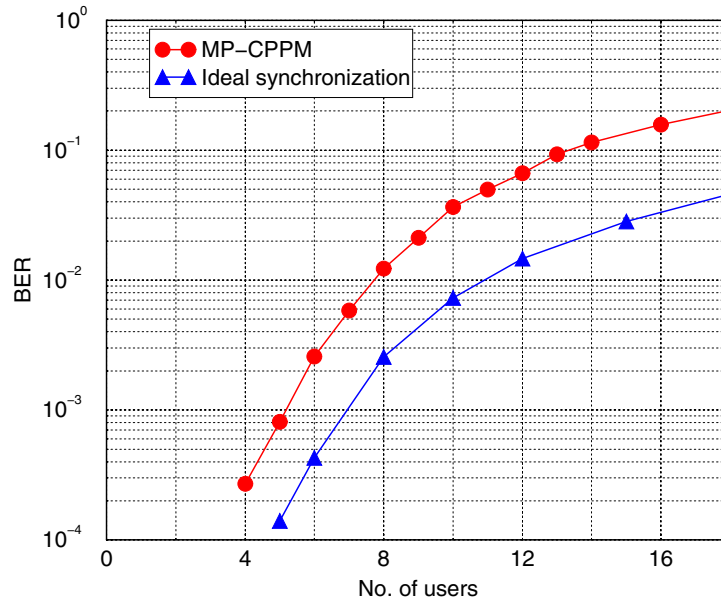


**Fig. 2.19.** Bit-error rate as a function of the number of users in a multipulse CPPM scheme. Circles correspond to the MP-CPPM, and triangles correspond to the standard (periodic) PPM scheme. (Reprinted with permission from [43], ©2001 IEEE.)

We tested this scheme in numerical simulations with up to 20 users. The pulse train patterns were chosen to minimize the maximum cross-correlation between different pulse trains. Chaotic intervals between the pulse trains were generated by the tent map with the slope 1.3. Then at the transmitter, the pulse train was produced either at time  $T_n - \delta$  or  $T_n + \delta$ , depending on the value (0 or 1, respectively) of bit  $b_n$  being transmitted. Unlike the single-pulse CPPM, the detection scheme is based on the position of the maximum output of the correlator within a certain window with respect to the nominal (determined by the chaotic clock) position  $T_n$ . If the pulse train arrival time is closer to  $T_n - \delta$  than to  $T_n + \delta$ , bit 0 is registered, and otherwise bit 1 is registered. We also employed an adjustable window size depending on the magnitude of the output from the matched filter, so when the signal is weak (synchronization is lost), the window becomes large in order to re-establish synchronization. Figure 2.19 shows the bit-error rate as a function of the number of users for 50-pulse trains. As was mentioned above, the performance of this system is degraded by occasional desynchronization events. For comparison, a corresponding plot for an ideally synchronized chaos oscillator at the receiver and transmitter is shown. As can be seen, the difference between these graphs is approximately 25% in terms of the number of users.

## 2.7 Conclusions

Discussing chaos-based communication systems, one may notice a potential disadvantage common to all such schemes utilizing synchronization. Most traditional schemes are based on periodic signals and carrier waveforms stored at the receiver and not transmitted through the channel. All such systems are characterized by zero Kolmogorov-Sinai entropy  $h_{KS}$  [46]: in these systems without any input the average rate of nonredundant information generation is zero. Chaotic systems have positive  $h_{KS}$  and continuously generate information. In the ideal environment, in order to perfectly synchronize two chaotic systems, one must transmit an amount of information per unit time that is equal to or larger than  $h_{KS}$  [46]. Although our detection method allows some tolerance in the synchronization precision, the need to transmit extra information to maintain the synchronization results in an additional shift of the actual CPPM performance curve relative to the case when ideal synchronization is assumed. Because the numerical and experimental curves in Figure 2.3 pass rather close to the analytical curve that assumes synchronization, the degradation caused by nonzero Kolmogorov-Sinai entropy does not seem to be significant.

Although CPPM performs slightly worse than BPSK, noncoherent FSK, and ideal PPM, we should emphasize that (i) this wideband system provides low probability of intercept and low probability of detection; (ii) improves the privacy while adding little circuit complexity; (iii) to our knowledge, this system performs exceptionally well compared to most other chaos-based covert

communication schemes; (iv) there exists a multiplexing strategy described above that can be used with CPPM (see also [47, 48]); and (v) compared to other impulse systems, CPPM does not rely on a periodic clock, and thus can eliminate any trace of periodicity from the spectrum of the transmitted signal. All this makes CPPM attractive for development of chaos-based communications.

## Acknowledgments

The authors are grateful to H.D.I. Abarbanel, L. Larson, L. Kocarev, and M.A. Vorontsov for helpful discussions. This work was supported in part by U.S. Department of Energy (grant DE-FG03-95ER14516), the U.S. Army Research Office (MURI grant DAAG55-98-1-0269). The authors also thank J. Gowens and J. Carrano for support in the development of the Atmospheric Laser Optics Testbed (A LOT) at Adelphi, Maryland used in the laser experiments.

## References

1. K. M. Cuomo and A. V. Oppenheim, Circuit implementation of synchronized chaos with applications to communications, *Phys. Rev. Lett.*, vol. 71(1), pp. 65–68, 1993.
2. L. Kocarev, K. S. Halle, K. Eckert, L. O. Chua and U. Parlitz, Experimental demonstration of secure communications via chaotic synchronization. *Int. J. Bifurcation Chaos*, vol. 2, pp. 709–713, 1992.
3. T. L. Carroll and L. M. Pecora, Synchronizing nonautonomous chaotic circuits, *IEEE Trans. Circuits Syst.*, vol. 40(10), pp. 646–650, 1993.
4. C. W. Wu and L. O. Chua, A simple way to synchronize chaotic systems with applications to secure communication systems, *Int. J. Bif. Chaos*, vol. 3(6), pp. 1619–1627, 1993.
5. P. Colet and R. Roy, Digital communication with synchronized chaotic lasers, *Optics Lett.*, vol. 19(24), pp. 2056–2058, 1994.
6. P. Celka, Chaotic synchronization and modulation of nonlinear time-delayed feedback optical systems. *IEEE Trans. Circuits Syst.*, vol. 42(8), pp. 455–463, 1995.
7. P. Celka, Synchronization of chaotic optical dynamical systems through 700 m of single mode fiber. *IEEE Trans. Circuits Syst.*, vol. 43(10), pp. 869–872, 1996.
8. C. R. Mirasso, P. Colet, and P. Garcia-Fernández, Photonics Technol. Lett **8**, 299 (1996)
9. G. D. VanWiggeren and R. Roy, Communication with chaotic lasers, *Science*, vol. 279(5354), pp. 1198–1200, 1998.
10. G. D. VanWiggeren and R. Roy, Optical communication with chaotic waveforms, *Phys. Rev. Lett.*, vol. 81(16), pp. 3547–3550, 1998.
11. H. D. I. Abarbanel and M. B. Kennel, Synchronizing high-dimensional chaotic optical ring dynamics, *Phys. Rev. Lett.*, vol. 80(14), pp. 3153–3156, 1998.

12. G. Kolumban, G. Kis, and Z. Jákó, M. P. Kennedy. FM-DCSK: a robust modulation scheme for chaotic communications. *IEICE Trans. Fundamentals of Electronics, Communication, and Computer Science*, vol.E81-A(9), pp. 1798–8002, 1998.
13. L. M. Pecora and T. L. Carroll. Synchronization in chaotic systems. *Phys. Rev. Lett.*, vol.64, pp. 821–824, 1990.
14. H. Fujisaka and T. Yamada, Stability theory of synchronized motion in coupled-oscillator systems, *Prog. Theor. Phys.*, vol. 69(1), pp. 32–47, 1984.
15. L. M. Pecora and T. L. Carroll, Synchronization in chaotic systems, *Phys. Rev. Lett.*, vol. 64(8), pp. 821–824, 1990.
16. D. R. Frey, Chaotic digital encoding: an approach to secure communication, *IEEE Trans. Circuits Syst.*, vol. 40(10), pp. 660–666, 1993.
17. A. R. Volkovskii and N. F. Rulkov, Synchronous chaotic response of a nonlinear oscillator system as a principle for the detection of the information component of chaos, *Tech. Phys. Lett.*, vol. 19(2), pp. 97–99, 1993.
18. U. Feldmann, M. Hasler, and W. Schwarz, Communication by chaotic signals: the inverse system approach, *Int. J. Circuit Theory Appl.*, vol. 24(5), 1996, pp. 551–579.
19. L. Kocarev and U. Parlitz, General approach for chaotic synchronization with applications to communication. *Phys. Rev. Lett.*, vol. 74(25), pp. 5028–5031, 1995.
20. M. Hasler. Synchronization of chaotic systems and transmission of information. *Int. J. of Bifurcation and Chaos*, vol. 8(4), pp. 647–659, 1998.
21. T. L. Carroll and L. M. Pecora, Cascading synchronized chaotic systems. *Physica D*, vol. 67, pp. 126–140, 1993.
22. H. Dedieu, M. P. Kennedy, and M. Hasler, Chaos shift keying: modulation and demodulation of a chaotic carrier using self-synchronizing Chua's circuits. *IEEE Trans. Circuits Syst. - I*, vol. 40, pp. 634–642, 1993.
23. K. Murali and M. Lakshmanan, Transmission of signals by synchronization in a chaotic Van der Pol-Duffing oscillator. *Phys. Rev. E*, vol. 48, pp. R1624–1626, 1993.
24. Y. H. Yu, K. Kwak, and T. K. Lim, Secure communication using small time continuous feedback. *Physics Letters A*, vol. 197, pp. 311–316, 1995.
25. K. S. Halle, C. W. Wu, M. Itoh, and L. O. Chua, Spread spectrum communication through modulation of chaos. *Int. J. Bifurcation Chaos*, vol. 3, pp. 469–477, 1993.
26. U. Parlitz and L. Kocarev, General approach for chaotic synchronization with applications to communication. *Phys. Rev. Lett.*, vol. 74, pp. 5028–5031, 1995.
27. U. Parlitz, L. Kocarev, T. Stojanovski, and H. Preckel, Encoding messages using chaotic synchronization. *Phys. Rev. E*, vol. 53, pp. 4351–4361, 1996.
28. N. F. Rulkov and L. S. Tsimring. Synchronization methods for communications with chaos over band-limited channel *Int. J. Circuit Theory and Applications.*, vol. 27, pp. 555–567, 1999.
29. G. Kolumban, M. P. Kennedy and L. O. Chua, The role of synchronization in digital communications using chaos. II. Chaotic modulation and chaotic synchronization, *IEEE Trans. Circuits Syst. - I*, vol. 45(11), pp. 1129–1140, 1998.
30. C. Williams, Chaotic communication over radio channels, *IEEE Trans. Circuits Syst. - I*, vol. 48(12), pp. 1394–1404, 2001.
31. T. L. Carroll, Amplitude-independent chaotic synchronization. *Phys. Rev. E*, vol. 53(4A), pp. 3117–3122, 1996.

32. T. L. Carroll and G. A. Johnson, Synchronizing broadband chaotic systems to narrow-band signals, *Phys. Rev. E*, vol. 57(2), pp. 1555–1558, 1998.
33. E. Rosa, S. Hayes, and C. Grebogi, Noise filtering in communication with chaos. *Phys. Rev. Lett.*, vol. 78(7), pp. 1247–1250, 1997.
34. N. F. Rulkov and A. R. Volkovskii, Threshold synchronization of chaotic relaxation oscillations, *Physics Letters A*, vol. 179(4-5), pp. 332–336, 1993.
35. H. Torikai, T. Saito, and W. Schwartz, Synchronization via multiplex pulse trains, *IEEE Trans. Circuits Syst. - I*, vol. 46(9), 1072–1085, 1999.
36. T. L. Carroll, Communicating with use of filtered, synchronized, chaotic signals, *IEEE Trans. Circuits Syst. - I*, vol. 42(2), pp. 105–110, 1995.
37. T. L. Carroll, Noise-robust synchronized chaotic communication, *IEEE Trans. Circuits Syst. - I*, vol. 48(12), pp. 1519–1522, 2001.
38. N. F. Rulkov and A. R. Volkovskii. Synchronization of pulse-coupled chaotic oscillators. In *Proc. of the 2nd Experimental Chaos Conference*, pp. 106–115, World Scientific, 1993.
39. M. M. Sushchik *et al.* Chaotic Pulse Position Modulation: a Robust Method of Communicating with Chaos *IEEE Communications Letters*, vol.4, pp. 128–130, 2000.
40. M. Z. Win and R. A. Scholtz. Impulse radio: how it works. *IEEE Communications Letters*, vol.2(2), pp.36–38, 1998.
41. T. Yang and L. O. Chua. Chaotic impulse radio: A novel chaotic secure communication system. *Int. J. of Bifurcation and Chaos*, vol.10, pp. 345–357, 2000.
42. P. A. Bernhardt Coupling of the relaxation and resonant elements in the autonomous chaotic relaxation oscillator (ACRO) *Chaos* vol.2, 183–199, 1992.
43. N. F. Rulkov, M. M. Sushchik, L. S. Tsimring, and A. R. Volkovskii Digital Communication Using Chaotic-Pulse-Position Modulation. *IEEE Trans. Circuits Syst.* vol. 48 , pp. 1436–1444, 2001.
44. N. F. Rulkov, M. A. Vorontsov and L. Illing Chaotic Free-Space Laser Communication over Turbulent Channel. *Phys. Rev. Lett.* vol. 89 , 277905, 2002.
45. L. C. Andrews, R. L. Phillips, and C. Y. Hopen, *Laser Beam Scintillation with Applications* (SPIE Press, Bellingham, 2001).
46. T. Stojanovski, Lj. Kocarev, and R. Harris. Applications of symbolic dynamics in chaos synchronization. *IEEE Trans. Circuit. Syst. I*, vol.44(10), pp. 1014–1017, 1997.
47. H. Torikai, T. Saito, and W. Schwarz. Multiplex communication scheme based on synchronization via multiplex pulse-trains. In *Proceedings of the 1998 IEEE International Symposium on Circuits and Systems*, pp. 554–557, New York, 1998.
48. H. Torikai, T. Saito, and W. Schwarz. Synchronization via multiplex pulse-trains. *IEEE Trans. Circuit. Syst. I*, vol.46(9), pp.1072–1085, 1999.

Digital Communications Using Chaos and Nonlinear  
Dynamics

Liu, J.-M.; Tsimring, L.S. (Eds.)

2006, XIV, 382 p. 196 illus., Hardcover

ISBN: 978-0-387-29787-3